

# Bayesian Optimization for QAOA

Simone Tibaldi,<sup>1, 2,\*</sup> Davide Vodola,<sup>1, 2</sup> Edoardo Tignone,<sup>3</sup> and Elisa Ercolessi<sup>1, 2</sup>

<sup>1</sup>*Dipartimento di Fisica e Astronomia dell’Università di Bologna, I-40127 Bologna, Italy*

<sup>2</sup>*INFN, Sezione di Bologna, I-40127 Bologna, Italy*

<sup>3</sup>*Leithà S.r.l. | Unipol Group, Bologna, Italy*

The Quantum Approximate Optimization Algorithm (QAOA) adopts a hybrid quantum-classical approach to find approximate solutions to variational optimization problems. Infact, it relies on a classical subroutine to optimize the parameters of a quantum circuit. In this work we present a Bayesian optimization procedure to fulfil this optimization task, and we investigate its performance in comparison with other global optimizers. We show that our approach allows for a significant reduction in the number of calls to the quantum circuit, which is typically the most expensive part of the QAOA. We demonstrate that our method works well also in the regime of slow circuit repetition rates, and that few measurements of the quantum ansatz would already suffice to achieve a good estimate of the energy. In addition, we study the performance of our method in the presence of noise at gate level, and we find that for low circuit depths it is robust against noise. Our results suggest that the method proposed here is a promising framework to leverage the hybrid nature of QAOA on the noisy intermediate-scale quantum (NISQ) devices.

## I. INTRODUCTION

Hybrid quantum-classical variational algorithms [1–3] play a central role in the current research on noisy intermediate-scale quantum (NISQ) devices [4]. In a hybrid variational setting, a classical computer is entrusted with the non-trivial task of optimizing the parameters of a quantum state. These algorithms implement a heuristic protocol to approximately solve variational problems including combinatorial optimization tasks, which are ubiquitous and have a great practical importance [5], and are indeed one of the main drivers of the industry interest towards quantum computing applications. Unfortunately, the problems belonging to this class are hard to solve with classical methods [6]. In this paper we focus on the Max-Cut and the Max Independent Set problems defined on specific graph instances.

Among the hybrid variational algorithms, the Quantum Approximate Optimization Algorithm (QAOA) [7] is extensively studied [8] as a promising algorithm to investigate quantum speedups on NISQ devices and has been implemented on several experimental platforms, such as Rydberg atom arrays [9], superconducting processors [10], trapped-ions simulators [11], as well as simulated on classical devices [12].

Similarly to other hybrid variational algorithms, QAOA consists in a sequence of parametrized quantum gates applied to a wavefunction, on which an expectation value of some operator, typically the Hamiltonian, is reconstructed from measurements. The task of the classical subroutine is to optimize the gate parameters in order to minimize such expectation value. Every variational quantum algorithm therefore requires the estimation of the wavefunction, which is a sub-optimal problem that requires resources that grow exponentially with the

system size [13]. Furthermore, the interplay between the classical and quantum parts of the algorithm entails to run the quantum circuit a large number of times, thus being expensive in term of resources.

To overcome these issues, an efficient classical optimization routine is crucial. Different techniques have been proposed for optimizing variational quantum circuits, e.g. Nelder-Mead [14], Monte-Carlo [15], gradient descent [16] and also Bayesian methods [17–20]. Here, we focus on a Bayesian optimization framework, which is suitable for gradient-free global optimization of black-box functions [21, 22]. We explore its behaviour in comparison with other global optimizers and we show that the convergence rate to a minimum is faster. We also demonstrate that the Bayesian approach is efficient in terms of number of circuit runs and is robust against noise sources.

The paper is structured as follows. In Section II we introduce the QAOA algorithm. In Section III we give a detailed presentation of the Bayesian algorithm. In Section IV we present the result of applying this method to QAOA, compare it to other global optimization methods, evaluate its performance with a limited number of circuit runs and against simulated quantum noise. Finally, in Section V we give the final remarks and comments.

## II. QAOA FOR COMBINATORIAL PROBLEMS

The QAOA is a variational quantum algorithm that performs hybrid quantum-classical optimization [7]. Given a cost function  $C(z)$  with  $z = (z_1, \dots, z_i, \dots, z_N)$  with  $z_i \in \{0, 1\}$ , QAOA aims at finding the bitstring  $z^*$  that minimizes the cost. In order to do so, the cost function is translated into a quantum operator  $H_C$  that is diagonal in the computational basis  $|z\rangle = |z_1 \dots z_i \dots z_N\rangle$  for  $N$  qubits i.e.  $H_C |z\rangle = C(z) |z\rangle$ .

The QAOA circuit consists in preparing an initial state of  $N$  qubits, usually  $|\psi\rangle = \sum_z |z\rangle / \sqrt{2^N}$ , and then applying two unitary operators alternatively: one generated

\* [simone.tibaldi2@unibo.it](mailto:simone.tibaldi2@unibo.it)

by  $H_C$ , the other generated by  $H_M = \sum_i X_i$ , where  $X_i$  is the flip (NOT) operator on the  $i$ -th for a number of layers  $p$  which is called the *depth* of the circuit. In this way the QAOA circuit prepares the state:

$$|\boldsymbol{\theta}\rangle = \prod_{l=1}^p e^{-i\beta_l H_M} e^{-i\gamma_l H_C} |\psi\rangle \quad (1)$$

where  $\boldsymbol{\theta} = (\boldsymbol{\gamma}, \boldsymbol{\beta})$  are  $2p$  parameters. By measuring the state  $|\boldsymbol{\theta}\rangle$  in the computational basis an estimate of the energy  $E(\boldsymbol{\theta}) = \langle \boldsymbol{\theta} | H_C | \boldsymbol{\theta} \rangle$  is obtained. This energy is fed to a classical routine which looks for the set of angles  $\boldsymbol{\theta}^* = (\boldsymbol{\gamma}^*, \boldsymbol{\beta}^*)$  that minimizes  $E(\boldsymbol{\theta})$ . Several strategies have been proposed for finding the optimal parameters  $\boldsymbol{\theta}^*$ . In this work we rely on Bayesian optimization.

### III. BAYESIAN OPTIMIZATION

Bayesian optimization is a global optimization strategy which allows one to find within relatively few evaluations the minimum of a noisy, black-box objective function  $f(\boldsymbol{\theta})$  that is in general expensive to evaluate [23]. The algorithm for the optimization method can be summarized as follows: (i) it treats the objective function  $f$  as a random function by choosing a prior (also called surrogate model) for  $f$ . Several choices for the surrogate model are possible [21], in this work we adopt the so-called Gaussian process [24]. (ii) The prior is then updated through the likelihood function by gathering observations of  $f$  and therefore forming the posterior distribution. (iii) The posterior distribution is finally used to construct an auxiliary function, called acquisition function, that is in general cheap to evaluate. The point where the acquisition function is maximized gives the next point where  $f$  will be evaluated [22].

Since Bayesian optimization requires no previous knowledge on  $f$ , it appears to be a well-suited technique for optimizing the parameters of a variational circuit running on NISQ devices.

In the following sections we describe the Gaussian process, the optimization routine and the acquisition function in detail.

#### A. Gaussian process

Since the function  $f(\boldsymbol{\theta})$  ( $\boldsymbol{\theta} \in A \subset \mathbb{R}^d$ ) to be optimized is unknown, we may think of it as belonging to a random process, i.e an infinite collection of random variables defined for every point  $\boldsymbol{\theta} \in A$ . A random process is called Gaussian if the joint distribution of any finite collection of those random variables is a multivariate normal distribution defined by a mean function  $\mu(\boldsymbol{\theta})$  and covariance (or kernel) function  $k(\boldsymbol{\theta}, \boldsymbol{\theta}')$  [24]. The mean function is related to the expected value of the function  $f$ , while the kernel estimates the deviations of the mean function from

the value of  $f$ :

$$\mu(\boldsymbol{\theta}) = \mathbb{E}[f(\boldsymbol{\theta})], \quad (2)$$

$$k(\boldsymbol{\theta}, \boldsymbol{\theta}') = \mathbb{E}[(f(\boldsymbol{\theta}) - \mu(\boldsymbol{\theta}))(f(\boldsymbol{\theta}') - \mu(\boldsymbol{\theta}'))], \quad (3)$$

where  $\mathbb{E}$  denotes the expectation value w.r.t. the infinite collection of functions belonging to the random process.

Since we assume  $f$  to be smooth, we choose Matérn kernel, that is a stationary kernel [24] that depends on the distance between the points  $\boldsymbol{\theta}$  and  $\boldsymbol{\theta}'$ :

$$k(\boldsymbol{\theta}, \boldsymbol{\theta}') = \sigma^2 \left( 1 + \frac{\sqrt{3} \|\boldsymbol{\theta} - \boldsymbol{\theta}'\|_2}{\ell} \right) e^{-\frac{\sqrt{3} \|\boldsymbol{\theta} - \boldsymbol{\theta}'\|_2}{\ell}} \quad (4)$$

where  $\|\cdot\|_2$  is the 2-norm and  $\sigma^2$  and  $\ell$  are two hyperparameters characterizing the Gaussian process. The hyperparameter  $\sigma^2$  defines the variance of the random variables whereas  $\ell$  is a characteristic length-scale which regulates the decay of the correlation between points: in the limit of  $\ell \rightarrow \infty$  all points are equally correlated, for  $\ell \rightarrow 0$  all points are uncorrelated.

#### B. Bayesian optimization

The main steps of the algorithm for Bayesian optimization can be summarized in the pseudocode in Algorithm 1. (See also Appendix A for details).

---

#### Algorithm 1: Pseudo-code for Bayesian optimization

---

```

Set the prior on  $f$  as a Gaussian process;
Evaluate  $f$  at  $N_W$  different points  $\boldsymbol{\theta}_i$ ;
Define the initial training set  $\mathcal{D} = \{(\boldsymbol{\theta}_i, f(\boldsymbol{\theta}_i))\}_{i=1}^{N_W}$ ;
Compute the hyperparameters  $\sigma, \ell$  based on  $\mathcal{D}$ ;
Set the guess for the minimum of  $f$  to
 $f_m = \min[\{f(\boldsymbol{\theta}_i)\}_{i=1}^{N_W}]$ ;
while  $n \leq N_{\text{BAYES}}$  do
    Update the posterior distribution on  $f$  using the
    training set  $\mathcal{D}$ ;
    Compute the acquisition function with the
    updated posterior;
    Find  $\tilde{\boldsymbol{\theta}}$  that maximizes the acquisition function;
    Evaluate  $f(\tilde{\boldsymbol{\theta}})$ ;
    if  $f(\tilde{\boldsymbol{\theta}}) < f_m$  then
        Set the guess for the minimum of  $f$  to
         $f_m = f(\tilde{\boldsymbol{\theta}})$ ;
    end
    Append  $(\tilde{\boldsymbol{\theta}}, f(\tilde{\boldsymbol{\theta}}))$  to  $\mathcal{D}$ ;
    Compute the new hyperparameters  $\sigma, \ell$ ;
    Increment  $n$ ;
end
return  $f_m$ 

```

---

The optimization starts by a warmup phase where a number  $N_W$  of evaluations of the objective function  $f$  is performed. These evaluations take place at random chosen values of the parameters  $\boldsymbol{\theta}_i$  and are collected in

the training set  $\mathcal{D} = \{(\boldsymbol{\theta}_i, y_i = f(\boldsymbol{\theta}_i))\}_{i=1}^{N_W}$  of the optimization. Given the set  $\mathcal{D}$ , we define the design matrix  $\boldsymbol{\Theta} = (\boldsymbol{\theta}_1, \dots, \boldsymbol{\theta}_{N_W})$  with the parameters, the vector  $\mathbf{y} \in \mathbb{R}^{N_W}$  with the observations via  $\mathbf{y} = (y_1, \dots, y_{N_W})$  and the covariance matrix  $\mathbf{K} \in \mathbb{R}^{N_W \times N_W}$  formed by evaluating the covariance function in Eq. (3) for each pair of points  $\boldsymbol{\theta}_i, \boldsymbol{\theta}_j \in \boldsymbol{\Theta}$  via

$$K_{i,j} = k(\boldsymbol{\theta}_i, \boldsymbol{\theta}_j) \quad (5)$$

where  $K_{i,j}$  denotes the  $(i, j)$  element of the matrix  $\mathbf{K}$ . The hyperparameters entering the kernel function (Eq.(2)) are optimized as explained in the following sec. III D.

The training set will be used at each step of the optimization for incorporating the acquired knowledge in the Gaussian process, by updating the prior distribution and thus for predicting the values of  $f$  at any point  $\boldsymbol{\theta} \in A$ . This prediction is done by conditioning the prior Gaussian process on the observations in  $\mathcal{D}$  [24] and returns a posterior distribution still described by a Gaussian process multinomial distribution characterized by a posterior mean  $\mu'$  and covariance  $k'$  that are given by

$$\mu' = \boldsymbol{\kappa}^T \cdot \mathbf{K}^{-1} \cdot \mathbf{y} \quad (6)$$

$$k' = k(\boldsymbol{\theta}, \boldsymbol{\theta}) - \boldsymbol{\kappa}^T \cdot \mathbf{K}^{-1} \cdot \boldsymbol{\kappa} \quad (7)$$

where  $\boldsymbol{\theta}$  is a generic point in  $A$ ,  $\boldsymbol{\kappa}$  is a column vector formed by evaluating the covariance function  $k$  between the generic point  $\boldsymbol{\theta}$  and all the points in  $\boldsymbol{\Theta}$ , i.e. its  $j$ -th element is  $\kappa_j = k(\boldsymbol{\theta}, \boldsymbol{\theta}_j)$ . Eq. (6) shows that the new mean is a linear combination of the observations  $\mathbf{y}$ .

### C. Acquisition Function

The next step in the Bayesian optimization is computing the acquisition function whose maximum gives the next point at which to evaluate the objective function. A common choice of acquisition function is the expected improvement that suggests to evaluate  $f$  in a point that, on average, improves on  $f_m$  the most [22]. This choice corresponds to defining the acquisition function  $\alpha(\boldsymbol{\theta}) = \mathbb{E}[u(\boldsymbol{\theta})]$  as the average value of the utility function  $u(\boldsymbol{\theta}) = \max[0, f_m - f(\boldsymbol{\theta})]$  such that the lower  $f(\boldsymbol{\theta})$  is with respect to the current minimum, the larger the utility  $u(\boldsymbol{\theta})$  will be.

By considering that  $f(\boldsymbol{\theta})$  is a Gaussian process, we can obtain an analytical expression for  $\alpha(\boldsymbol{\theta})$  as

$$\alpha(\boldsymbol{\theta}) = \Phi(z)(f_m - \mu') + \phi(z)k' \quad (8)$$

where  $\mu'$  and  $k'$  are obtained for the point  $\boldsymbol{\theta}$  by using Eqs. (6) and (7);  $\Phi(\cdot)$  and  $\phi(\cdot)$  are the cumulative distribution function and the probability density function, respectively, of the standard normal distribution and the quantity  $z$  is defined as  $z = (f_m - \mu')/k'$ . The two terms in Eq. (8) resume the trade-off between exploitation and exploration: the first term, being proportional to the difference between the current minimum and the mean value

of the posterior, brings the optimization towards points with lower  $\mu'$  whereas the second one promotes points with larger  $k'$ , i.e. with higher uncertainty.

In this work, we compute the point  $\tilde{\boldsymbol{\theta}}$  that maximizes the acquisition function by using the differential evolution algorithm [25], a population-based metaheuristic search algorithm (see Appendix C for details).

### D. Hyperparameters

We are now only left with the task of picking the best hyperparameters  $\sigma, \ell$  for the Matérn kernel. This is typically done by considering the marginal likelihood [24]

$$p(\mathbf{y}|\boldsymbol{\Theta}) = \int p(\mathbf{y}|\mathbf{f}, \boldsymbol{\Theta})p(\mathbf{f}|\boldsymbol{\Theta})d\mathbf{f} \quad (9)$$

where the prior  $p(\mathbf{f}|\boldsymbol{\Theta})$  and the likelihood  $p(\mathbf{y}|\mathbf{f}, \boldsymbol{\Theta})$  are Gaussian and the marginalization is done over the function values  $\mathbf{f}$ . Given the Gaussian nature of the likelihood and the prior, a closed form of the log marginal likelihood can be obtained (for more details see [24]):

$$\log p(\mathbf{y}|\boldsymbol{\Theta}) = -\frac{1}{2}\mathbf{y}^T \cdot \mathbf{K}^{-1} \cdot \mathbf{y} - \frac{1}{2}\log \det \mathbf{K} - \frac{N}{2}\log 2\pi, \quad (10)$$

where  $N$  is the number of observations in the design matrix  $\boldsymbol{\Theta}$ . In Eq. (10), the first term specifies how well the process fits the data, the second term instead acts as a regularization factor on the elements of the kernel matrix. When fitting the Gaussian process to a new set of points, the best hyperparameters  $(\tilde{\sigma}^2, \tilde{\ell})$  can be found by maximizing the log marginal likelihood in Eq. (10). For the optimization of  $\log p(\mathbf{y}|\boldsymbol{\Theta})$ , we use the quasi-Newton method L-BFGS [26] with multiple restarting points which proved to be efficient on the flat landscape of the likelihood (see Appendix A for details).

## IV. RESULTS

In this section we apply the Bayesian optimization to the QAOA parameters. We consider two well-known combinatorial problems defined on graphs, the Max-Cut and the MIS.

*Max-Cut* – Given a graph  $G = (V, E)$  where  $V$  is the set of nodes and  $E$  the set of edges, the Max-Cut problem consists in finding a partition of the graph's vertices  $V$ ,  $P = \{V_0, V_1\}$ , such that the number of edges between  $V_0$  and its complement  $V_1$  is as large as possible. It is known to be a NP-hard problem [27]. Without loss of generality, one could think of labeling with label “1” the nodes  $v \in V_1$  and with label “0” the nodes  $v \in V_0$ . In these terms, the Max-Cut consists in finding the largest number of edges connecting a bit off (0) to a bit on (1). On a quantum computer every node of the graph is represented by a qubit, on which the measurement of the

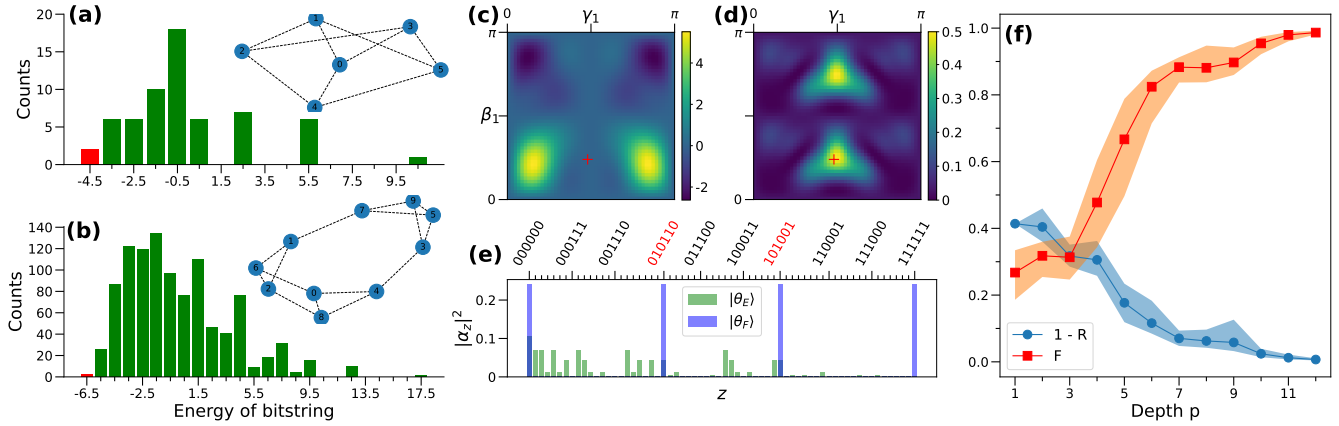


FIG. 1. **QAOA at low vs. large depth.** (a) Distribution of the energies of the possible bitstrings for the graph of 6 nodes (shown in the inset). The red bar highlights the two solution bitstrings of the MIS problem on such graph. (b) Distribution of the energies of the possible bitstrings for the graph of 10 nodes (shown in the inset). The red bar highlights the two solution bitstrings of the Max-Cut problem on such graph. (c) Landscape of the energy  $E(\theta_1)$  obtained on the 6 nodes graph solving the MIS problem. The red cross indicates the angles corresponding to the final state with largest fidelity,  $|\theta_F\rangle$ . (d) Landscape of the fidelity  $F(\theta_1)$ . (e) Squared amplitudes of the two states  $|\theta_E\rangle$ ,  $|\theta_F\rangle$ . The solution bitstrings are highlighted in red. (f) Average approximation ratio (plotted as  $1 - R$ ) and fidelity for increasing values of circuit depth from 1 to 12 over 50 runs. Shaded areas are the standard deviation.

Pauli gate  $Z$  returns  $\pm 1$ , so the cost Hamiltonian can be written as:

$$H_C^{\text{MC}} = - \sum_{(i,j) \in E} (1 - Z_i Z_j)/2 \quad (11)$$

*MIS* – The Max Independent Set problem consists in finding the largest number of graph nodes which are not adjacent, and the corresponding cost Hamiltonian is:

$$H_C^{\text{MIS}} = - \sum_i Z_i + \omega \sum_{(i,j) \in E} Z_i Z_j, \quad (12)$$

with  $\omega$  a parameter that balances the effect of the first term (maximizing the number of activate bits) and the second one (prevents neighbour bits to activate at the same time), set to 2 for the rest of the work.

For a graph with  $N$  nodes, the variational state prepared by the QAOA circuit is a superposition of all the  $2^N$  bitstrings,  $|\theta\rangle = \sum_z \alpha_z |z\rangle$ . The Bayesian optimization aims at finding the set of parameters  $\theta^*$  that maximize the coefficient  $\alpha_{z^*}$  where  $z^*$  is the solution of the combinatorial problem.

During the optimization process we monitor the approximation ratio  $R = E(\theta)/E_{GS}$  where  $E_{GS}$  is the energy of the solution bitstring. We also look at the fidelity defined as  $F = |\langle \theta | z^* \rangle|^2$  where  $|z^*\rangle$  is the state which encodes the solution. The results were obtained on two 3-regular graphs of 6 and 10 nodes respectively, plotted in the insets of Figs. 1(a)-(b).

*QAOA at low vs. large depth*– We start by looking at the QAOA at depth  $p = 1$  for the 6 nodes graph. It corresponds to a shallow circuit that depends only on two parameters  $\theta_1 = (\gamma_1, \beta_1)$ . We consider the MIS, and

we plot the landscapes of both the energy  $E(\theta_1)$  and the fidelity  $F(\theta_1)$  (Fig. 1(c) and (d), respectively) for values of  $\gamma_1, \beta_1 \in [0, \pi]$  due to the symmetry of the problem. We see that the landscape of the energy, which is the function to minimize, is rather flat with from two global maxima and minima, corresponding to the best solutions possible at  $p = 1$ .

Interestingly, we find that the QAOA state corresponding to the parameters which minimize the energy,  $|\theta_E\rangle$ , is not the state with largest fidelity,  $|\theta_F\rangle$ . To see how they differ we plot the squared amplitudes of both states in Fig. 1(e) as histograms. The fidelity of  $|\theta_F\rangle$  is, as expected, much larger than that one of  $|\theta_E\rangle$ , yet the latter has a lower energy because it has many non zero amplitudes along excited states with low energy. This unravels the problem of optimizing the QAOA parameters by only looking at the energy  $E(\theta)$ . There is a large concentration of excited states with energy comparable to the energy of the ground state, as shown in the histograms of panels (a) and (b) of Fig. 1. It is difficult to increase the amplitude corresponding to the solution when many other states can contribute with low values of the energy.

The divergence between lowest energy and highest fidelity is guaranteed to disappear theoretically for  $p \rightarrow \infty$ . For this reason, we show in Fig. 1(f) that the approximation ratio and fidelity both tend to 1 for  $p \sim 12$  already. Yet, we already see a good performance at  $p = 4$  where  $R > 0.7$  and we have  $F \sim 0.5$  meaning that more than 50% chance of measuring the solution on the state obtained with QAOA.

*Comparing resources*– Increasing the depth of a variational circuit increases the number of parameters that must be optimized. This, in turn, is expected to increase the number of calls to the quantum circuit needed to

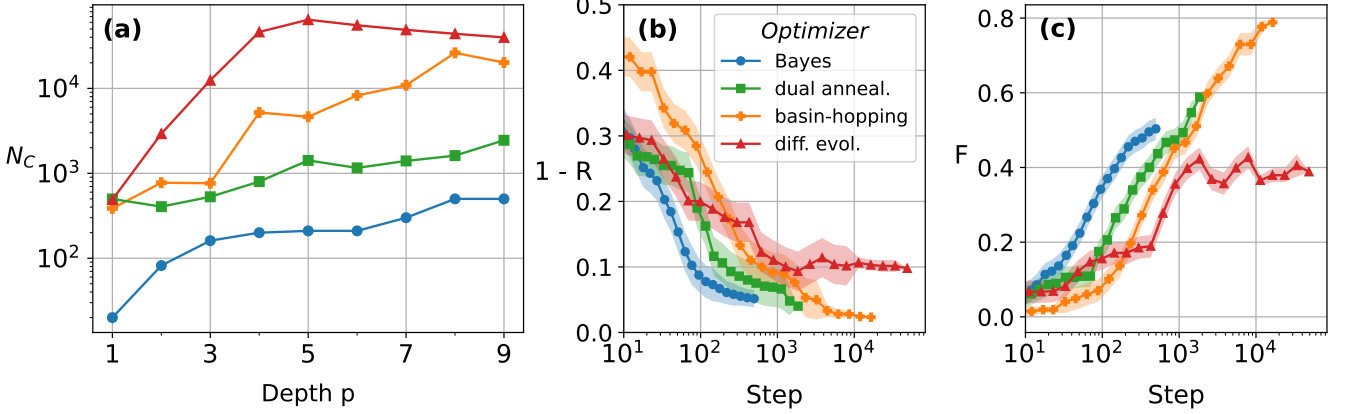


FIG. 2. **Comparison among optimizers.** (a) The plot shows the average number of calls  $N_C$  to the quantum circuit of each optimizer in order to obtain the same approximation ratio as the Bayesian optimization. (b) - (c) Average approximation ratio (plotted as  $1 - R$ ) and fidelity during optimization for the different methods at  $p = 7$  over 30 runs. Shaded areas represent the standard deviation.

reach a good approximate solution, which is a problem in the current NISQ era, since running a quantum circuit can be costly due to both state preparation routines and recalibrations of the device.

Bayesian optimization mitigates such problem, and allows to achieve a good approximate solution within relatively fewer calls to the circuit compared to other global optimization methods (see Appendix D for details). To show this, we ran the optimizers on the 10 nodes graph of Fig. 1(b) for the Max-Cut problem at different depths. Fig. 2(a) shows the average number of calls to the circuit that the other optimizers need in order to reach the same approximation ratio of Bayesian optimization. To gain more insight, we plot in panels (b) and (c) of Fig. 2 the average approximation ratio and fidelity during the run of the algorithm for each method at  $p = 7$ . We see that Bayesian optimization stops at a lower  $R$  than basin-hopping and dual annealing, but it reaches a value of  $R = 95\%$  with 500 runs of the circuit compared to the other two methods which take, in order, 1400 and 10800.

*Slow Measurements* – The energy  $E(\boldsymbol{\theta})$  is obtained by measuring the QAOA state after running the circuit: we refer to these two operations combined together as a “shot”. By measuring on the  $Z$  basis at each shot we get a bitstring, and we calculate its classical energy associated to the combinatorial problem. The precision in the reconstruction of  $E(\boldsymbol{\theta})$  depends on the number of shots  $N_S$ . Since we consider this as a multinomial sampling problem we expect the variance of the reconstructed energy to depend on  $N_S^{-1}$ . In many scenarios of NISQ devices it is necessary to balance  $N_S$  with the desired standard deviation. For this reason, we compare the average approximation ratio obtained with the exact energy (simulated) with the energy reconstructed with a limited number of shots.

We show in Fig. 3 such comparison with a number of shots  $N_S$  equal to, respectively, 1024, 128, 64, 16, 4.

Looking at the approximation ratio  $R$  (Fig. 3(a)) we see that taking  $N_S = 128$  shots reduces  $R$  by 5% respect to  $N_S = 1024$  and going to  $N_S = 64$  reduces it by a further 5%. This behaviour then stops and even reverses its trend. Infact, we even see an average increase going from  $N_S = 16$  to 4 respectively. That is due to the fact that such few measurements cannot give a precise estimate of the energy. An analogous behaviour can be found in the fidelity, panel (b) of Fig. 3.

To have a better understanding of how the algorithm adapts to the sampling noise, we look at the kernel noise parameter which is learned by the Gaussian process during the fitting, at each step of the optimization (see Appendix B for details on the noise hyperparameter). The plot in Fig. 3(c) shows that, after an initial phase, the kernel noise sets at a specific value at around 400 steps. In addition to that, the lower the number of shots the larger the noise parameters learned. In fact, by fitting the average kernel noise found at the end of the training (Fig. 3(d)) we obtain a power law with  $N_S^{-1.1}$ . This trend is comparable to the expected trend for the variance  $N_S^{-1}$  of the reconstruction of the energy. This shows that the Gaussian process can account for noise.

*Quantum noise* – Another relevant issue in the state-of-the-art NISQ devices are the sources of quantum noise which can interfere with the quantum circuit. Every device has different sources of noise depending on the underlying technology. In order to simulate it without specifying the device technology we add random noise on every QAOA parameter. In this way eq. (1) is modified as:

$$|\boldsymbol{\theta}\rangle = \prod_{l=1}^p e^{-i \sum_i \beta_l^i X_i} e^{i \sum_i Z_i - i \sum_{\langle i,j \rangle} \gamma_l^{(i,j)} Z_i Z_j} |\psi\rangle \quad (13)$$

where  $\beta_l^i$  and  $\gamma_l^{(i,j)}$  act differently on every qubit/edge

of the graph at every layer because they are both perturbed by a random Gaussian noise with standard deviation  $\sigma_N$ . In Fig. 4 we compare different values of  $\sigma_N$  for different values of circuit depth  $p$  on the 10 nodes graph for the Max-Cut problem. By increasing  $\sigma_N$  and  $p$ , we expect to obtain a worse approximation ratio  $R$  because the error accumulates along the circuit as number of parameters grows. Indeed, as we can see in the figure, from  $p \geq 5$  the obtained  $R$  decreases w.r.t. the noiseless case, decreasing even by 20% for  $p = 9$  with  $\sigma_N$ . For  $p \leq 3$ , however,  $R$  increases with  $p$ , which indicates that, for shallow circuits, Bayesian optimization is robust against noise. Interestingly, for  $p = 1, 3$  we see that, on average, the obtained ratio is even better than the one obtained without noise.

## V. CONCLUSIONS

In this work we presented the Bayesian optimization algorithm as a subroutine to optimize the variational parameters of the QAOA. We applied it to find the solutions of two combinatorial optimization problems, the Max-Cut and the MIS on two graph instances. We started by introducing the QAOA, then we showed the details of the Bayesian optimization algorithm. We focused on its capability to adapt to the data and to predict new possible optimal points by exploiting both the accumulated knowledge and the uncertainty with respect to the optimization landscape.

In the results we analyzed some details of the QAOA at low circuit depth with the purpose of presenting some of the issues related to the optimization of a variational quantum algorithm. These include the flatness of the energy landscape and the limited information that we can

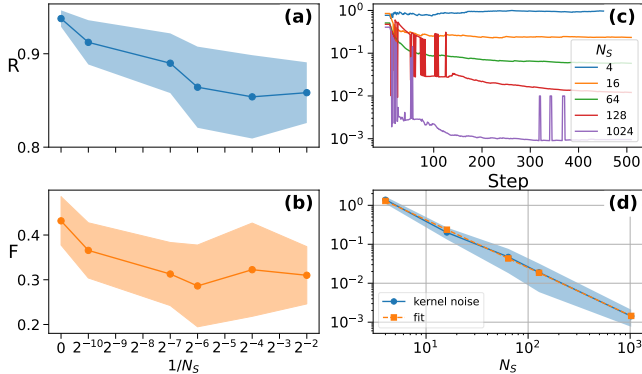


**FIG. 3. Slow measurements.** (a)-(b) Average approximation ratio and fidelity for decreasing number of shots. The  $1/N_S = 0$  shots indicates the exact energy. Shaded areas are the standard deviations. (c) Kernel noise learned by fitting during optimization for different number of shots  $N_S$ . (d) Average kernel noise learned by the Gaussian process for different values of  $N_S$ , the plot also shows the linear fit on the logarithmic data.

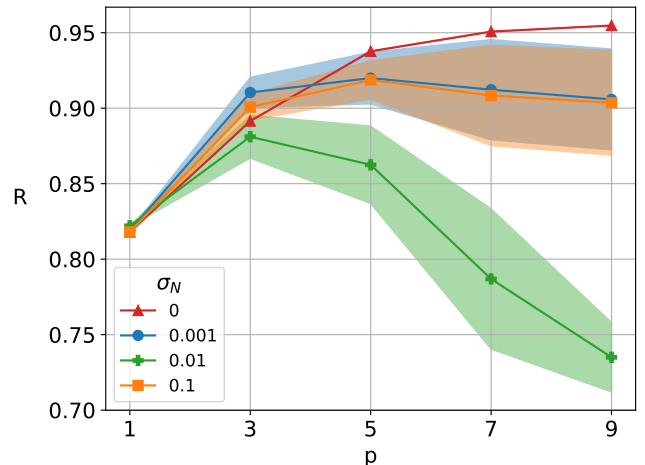


**FIG. 4. Quantum noise simulation.** The noise is simulated by adding random normal rotations to the parameters  $(\gamma, \beta)$  distributed with standard deviation  $\sigma_N$ . The plot shows, for increasing depth  $p$ , the effect of different intensities of noise. Shaded areas are the standard deviations.

retain from the energy of the QAOA state compared to its overlap with the ground state. After that, we compared Bayesian optimization with other global optimization methods, and we showed that they require many more calls, in the order of tens or hundreds, to the quantum circuit. This is a first sign that this method responds more efficiently to the requirements from the quantum part of the QAOA.

Secondly, we lowered the number of shots for the reconstruction of the energy. We showed that the results are slightly altered by a 5% decrease in the approximation ratio by using 1024 shots compared to optimization with the exact energy. We also lowered to 64, 16 and 4 shots and showed that in all the three cases the optimization is possible at the cost of a decrease in the approximation ratio by 10%. We also showed that the Gaussian process learns to add a noise hyperparameter which is proportional to the variance expected from the reconstruction of the energy. This can be seen as a further example of adaptation of the Bayesian algorithm to the data.

Finally, we simulated a source of noise and we showed that for shallow circuits,  $p \in [1, 3]$ , the approximation ratio is improved even for large standard deviations of noise. Yet, as expected, for deeper circuit,  $p \geq 5$ , the intensity of noise sensibly affects the final approximation ratio.

These findings show that Bayesian optimization is a robust method which can account for both quantum and sampling noise. For this reason it represents a valid tool for solving optimization problems via a hybrid algorithm to be run on a NISQ device.

## ACKNOWLEDGMENTS

We thank C. Sanavio and F. Dell’Anna for useful discussions. This research is funded by the International Foundation Big Data and Artificial Intelligence for Human Development (IFAB) through the project

“Quantum Computing for Applications”. E. Ercolessi, S. Tibaldi and D. Vodola are partially supported by Istituto Nazionale di Fisica Nucleare (INFN) through the project “QUANTUM” and the QuantERA 2020 Project “QuantHEP”.

---

[1] J. R. McClean, J. Romero, R. Babbush, and A. Aspuru-Guzik, *The theory of variational hybrid quantum-classical algorithms*, *New Journal of Physics* **18**, 023023 (2016).

[2] A. Peruzzo, J. McClean, P. Shadbolt, M.-H. Yung, X.-Q. Zhou, P. J. Love, A. Aspuru-Guzik, and J. L. O’Brien, *A variational eigenvalue solver on a photonic quantum processor*, *Nature Communications* **5**, 4213 (2014).

[3] N. Moll, P. Barkoutsos, L. S. Bishop, J. M. Chow, A. Cross, D. J. Egger, S. Filipp, A. Fuhrer, J. M. Gambetta, M. Ganzhorn, A. Kandala, A. Mezzacapo, P. Müller, W. Riess, G. Salis, J. Smolin, I. Tavernelli, and K. Temme, *Quantum optimization using variational algorithms on near-term quantum devices*, *Quantum Science and Technology* **3**, 030503 (2018).

[4] J. Preskill, *Quantum Computing in the NISQ era and beyond*, *Quantum* **2**, 79 (2018).

[5] D. Du and P. M. Pardalos, eds., *Handbook of Combinatorial Optimization* (Springer, 1999).

[6] M. R. Garey and D. S. Johnson, *Computers and Intractability: A Guide to the Theory of NP-Completeness* (W. H. Freeman, 1979).

[7] E. Farhi, J. Goldstone, and S. Gutmann, *A Quantum Approximate Optimization Algorithm*, (2014), arXiv:1411.4028.

[8] L. Zhou, S.-T. Wang, S. Choi, H. Pichler, and M. D. Lukin, *Quantum Approximate Optimization Algorithm: Performance, Mechanism, and Implementation on Near-Term Devices*, *Phys. Rev. X* **10**, 021067 (2020).

[9] S. Ebadi *et al.*, *Quantum optimization of maximum independent set using Rydberg atom arrays*, *Science* **376**, 1209 (2022).

[10] M. P. Harrigan, K. J. Sung, M. Neeley, K. J. Satzinger, F. Arute, K. Arya, J. Atalaya, J. C. Bardin, R. Barends, S. Boixo, and et al., *Quantum approximate optimization of non-planar graph problems on a planar superconducting processor*, *Nature Physics* **17**, 332 (2021).

[11] G. Pagano, A. Bapat, P. Becker, K. S. Collins, A. De, P. W. Hess, H. B. Kaplan, A. Kyriyanidis, W. L. Tan, C. Baldwin, L. T. Brady, A. Deshpande, F. Liu, S. Jordan, A. V. Gorshkov, and C. Monroe, *Quantum approximate optimization of the long-range Ising model with a trapped-ion quantum simulator*, *Proceedings of the National Academy of Sciences* **117**, 25396 (2020).

[12] M. Medvidović and G. Carleo, *Classical variational simulation of the Quantum Approximate Optimization Algorithm*, *npj Quantum Information* **7**, 101 (2021).

[13] M. Cramer, M. B. Plenio, S. T. Flammia, R. Somma, D. Gross, S. D. Bartlett, O. Landon-Cardinal, D. Poulin, and Y.-K. Liu, *Efficient quantum state tomography*, *Nature Communications* **1**, 149 (2010).

[14] G. G. Guerreschi and M. Smelyanskiy, *Practical optimization for hybrid quantum-classical algorithms*, (2017), arXiv:1701.01450 [quant-ph].

[15] D. Wecker, M. B. Hastings, and M. Troyer, *Training a quantum optimizer*, *Phys. Rev. A* **94**, 022309 (2016).

[16] Z. Wang, S. Hadfield, Z. Jiang, and E. G. Rieffel, *Quantum approximate optimization algorithm for MaxCut: A fermionic view*, *Phys. Rev. A* **97**, 022304 (2018).

[17] J. S. Otterbach *et al.*, *Unsupervised Machine Learning on a Hybrid Quantum Computer*, (2017), arXiv:1712.05771 [quant-ph].

[18] D. Zhu, N. M. Linke, M. Benedetti, K. A. Landsman, N. H. Nguyen, C. H. Alderete, A. Perdomo-Ortiz, N. Korda, A. Garfoot, C. Brecque, L. Egan, O. Perdomo, and C. Monroe, *Training of quantum circuits on a hybrid quantum computer*, *Science Advances* **5**, eaaw9918 (2019).

[19] C. N. Self, K. E. Khosla, A. W. R. Smith, F. Sauvage, P. D. Haynes, J. Knolle, F. Mintert, and M. S. Kim, *Variational quantum algorithm with information sharing*, *npj Quantum Information* **7**, 116 (2021).

[20] G. Wang, D. E. Koh, P. D. Johnson, and Y. Cao, *Minimizing Estimation Runtime on Noisy Quantum Computers*, *PRX Quantum* **2**, 010346 (2021).

[21] B. Shahriari, K. Swersky, Z. Wang, R. P. Adams, and N. de Freitas, *Taking the Human Out of the Loop: A Review of Bayesian Optimization*, *Proceedings of the IEEE* **104**, 148 (2016).

[22] P. I. Frazier, *A Tutorial on Bayesian Optimization*, (2018), arXiv:1807.02811 [stat.ML].

[23] J. Snoek, H. Larochelle, and R. P. Adams, *Practical Bayesian Optimization of Machine Learning Algorithms*, in *Advances in Neural Information Processing Systems*, Vol. 25, edited by F. Pereira, C. J. C. Burges, L. Bottou, and K. Q. Weinberger (Curran Associates, Inc., 2012).

[24] C. E. Rasmussen and C. K. I. Williams, *Gaussian Processes for Machine Learning (Adaptive Computation and Machine Learning)* (The MIT Press, 2005).

[25] K. Price, R. M. Storn, and J. A. Lampinen, *Differential evolution: a practical approach to global optimization* (Springer Science & Business Media, 2006).

[26] D. C. Liu and J. Nocedal, *On the limited memory BFGS method for large scale optimization*, *Mathematical Programming* **45**, 503 (1989).

[27] C. S. Edwards, *Some Extremal Properties of Bipartite Subgraphs*, *Canadian Journal of Mathematics* **25**, 475 (1973).

[28] D. J. Wales and J. P. K. Doye, *Global Optimization by Basin-Hopping and the Lowest Energy Structures of Lennard-Jones Clusters Containing up to 110 Atoms*, *The Journal of Physical Chemistry A* **101**, 5111 (1997).

[29] Y. Xiang, D. Sun, W. Fan, and X. Gong, *Generalized simulated annealing algorithm and its application to the Thomson model*, *Physics Letters A* **233**, 216 (1997).

## Appendix A: Details on the Bayesian optimization

In this appendix we give a detailed review of the algorithm we used in this work for performing the Bayesian optimization for the QAOA.

### 1. Bayesian optimization algorithm

This algorithm is made out of three phases: warmup, kernel optimization, acquisition function maximization and is summarized in Algorithm 1.

*Warmup*— In the warmup phase we start with a set of  $N_W = 10$  points  $X = \{\boldsymbol{\theta}_j\}_{j=1}^{N_W}$  with  $\boldsymbol{\theta}_j \in \mathbb{R}^d$  where  $d = 2p$  and  $p$  is the depth of the QAOA circuit, each point is a set of angles  $(\boldsymbol{\gamma}, \boldsymbol{\beta})$ . These points are sampled from the latin hypercube of bounds  $[0, \pi]^d$ . For each set of angles we estimate the energy of QAOA  $y_i$  and we create the design matrix  $\boldsymbol{\Theta} = (\boldsymbol{\theta}_1, \dots, \boldsymbol{\theta}_{N_W})$  and the observation vector  $\mathbf{y}$  with the energies of the points  $\boldsymbol{\theta}_j$ . We also store the point with lowest energy as  $(\boldsymbol{\theta}_m, f_m)$ .

*Kernel optimization*— In this part we look for the hyperparameters  $(\tilde{\sigma}, \tilde{\ell})$  which maximize the likelihood function  $p(\mathbf{y}|\boldsymbol{\Theta})$  (Eq. (10)). This optimization is performed by repeating the L-BFGS [26] minimization on  $-p(\mathbf{y}|\boldsymbol{\Theta})$  for 10 times and selecting the best parameters found. The parameters found at every step of the optimization are plotted in panels (c) and (d) of Fig. 6.

*Acquisition function maximization*— Once the hyperparameters are set the algorithm exploits its knowledge and uncertainty of the data to propose a new point  $\boldsymbol{\theta}'$  with the new parameters where we evaluate the QAOA circuit. This is done by maximizing the expected improvement in Eq. (8).

The new point  $\boldsymbol{\theta}'$  maximizing the expected improvement is then added to the dataset  $\mathcal{D}$  and the algorithm is repeated. The procedure stops after  $N_{\text{BAYES}}$  iterations. Fig. 5 provides an illustrative example (with  $p = 1$ ,  $N_W = 5$ , and  $N_{\text{BAYES}} = 20$ ) of how the Bayesian method operates and moves through the landscapes.

## Appendix B: Bayesian Optimization with noise

In this paper we consider two scenarios in which the energy  $E(\boldsymbol{\theta})$  is affected by a source of noise: the finite number of samplings and the quantum noise at the gate level. In the context of Bayesian optimization we can account for noise by modifying the kernel function adding a term like so:

$$k(\boldsymbol{\theta}, \boldsymbol{\theta}') = \sigma^2 \left( 1 + \frac{\sqrt{3} \|\boldsymbol{\theta} - \boldsymbol{\theta}'\|_2}{\ell} \right) e^{-\frac{\sqrt{3} \|\boldsymbol{\theta} - \boldsymbol{\theta}'\|_2}{\ell}} + \sigma_N^2 \mathbb{I} \quad (\text{B1})$$

This is usually called a White kernel and it is a parameter added to the diagonal to account for random fluctuations around the true value of  $f(\boldsymbol{\theta})$ . In this way

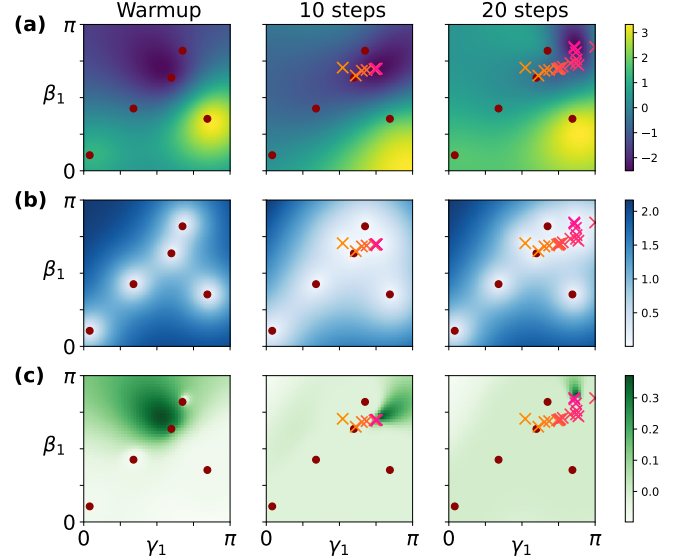


FIG. 5. **Posterior and acquisition function during optimization.** The image shows the predicted mean  $\mu'$  (a), the predicted variance  $k'$  (b) and the acquisition function  $\alpha(\boldsymbol{\theta})$  (c) (see Eqs. (6) - (8)) at three moments of the bayesian optimization of QAOA with  $p = 1$ , i.e.  $\boldsymbol{\theta} = (\gamma_1, \beta_1)$ . The red dots indicate the warmup points ( $N_W = 5$ , in this case) while the crosses are the points chosen by the algorithm (colored from first to last). At every step,  $\mu'$  shows the knowledge of the landscape of the function to optimize,  $k'$  shows the uncertainty while  $\alpha(\boldsymbol{\theta})$  combines the two to propose the next possible optimal point. The longer the optimization goes on, the more we see that  $k'$  is close to zero in larger areas while  $\alpha(\boldsymbol{\theta})$  becomes flat almost anywhere except for a small area. This means that the optimization is not exploring new areas any more and has enough acquired knowledge from the data to converge to the minimum.

the new predicted mean and covariance for a set of data  $\boldsymbol{\Theta}$  can be easily calculated to be:

$$\mu' = \boldsymbol{\kappa}^T \cdot (\mathbf{K} + \sigma_N^2 \mathbb{I})^{-1} \cdot \mathbf{y} \quad (\text{B2})$$

$$k' = k(\boldsymbol{\theta}, \boldsymbol{\theta}) - \boldsymbol{\kappa}^T \cdot (\mathbf{K} + \sigma_N^2 \mathbb{I})^{-1} \cdot \boldsymbol{\kappa} \quad (\text{B3})$$

The constant  $\sigma_N^2$  belongs to the list of hyperparameters (along with  $\sigma^2$  and  $\ell$ ) that are optimized with the log marginal likelihood which now takes the form

$$\begin{aligned} \log p(\mathbf{y}|\boldsymbol{\Theta}) = & -\frac{1}{2} \mathbf{y}^T \cdot (\mathbf{K} + \sigma_N^2 \mathbb{I})^{-1} \cdot \mathbf{y} \\ & -\frac{1}{2} \log \det(\mathbf{K} + \sigma_N^2 \mathbb{I}) \\ & -\frac{N}{2} \log 2\pi, \end{aligned}$$

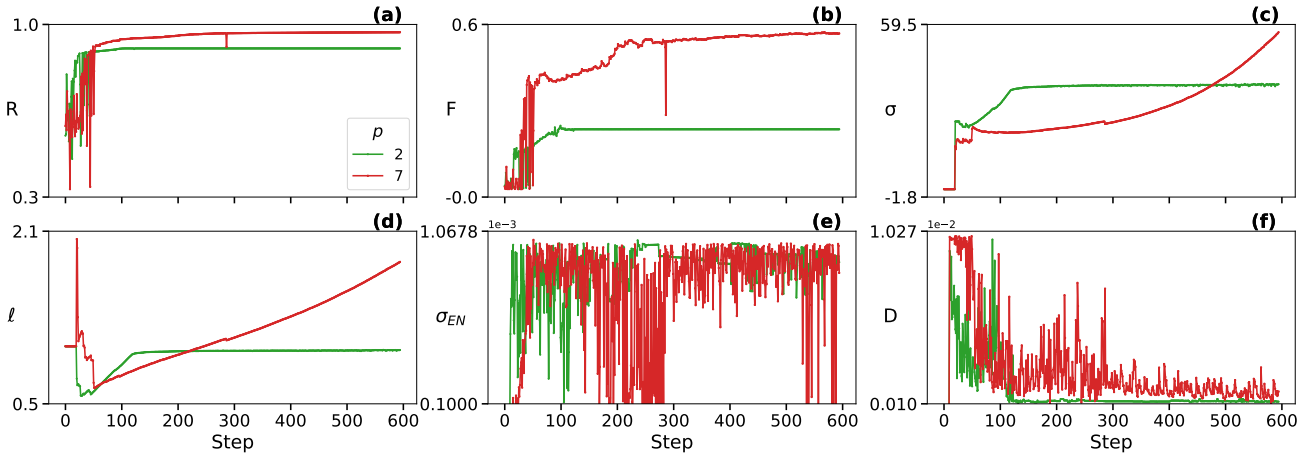


FIG. 6. **Parameters of Bayesian optimization at  $p = 2, 7$ .** Plots of the parameters changing during Bayesian optimization for two runs with  $N_{BAYES} = 600$  steps. (a) Approximation ratio  $R$ . (b) Fidelity. (c) Kernel constant. (d) Kernel correlation length. (e) Standard deviation of the energy of the points of differential evolution. (f) Average distance of the points of differential evolution.

### Appendix C: Differential evolution

The expected improvement can have a fairly flat landscape [23], especially at the beginning, due to the lack of observations. To reach its maximum we relied on the differential evolution [25], an evolutionary method in which, at each iteration, a population of points is obtained from the previous one in order to collectively converge to an optimal point.

The first population consists of  $N_P = 15 \cdot 2p$  points randomly selected on the latin  $2p$ -cube of bounds  $[0, \pi]^{2p}$ . Each point has an expected improvement  $EI(\theta_{i,1})$ , where  $i \in \{1, \dots, N_P\}$  uniquely identifies the point within the belonging population, while 1 indicates that the point belongs to the first generation.

At every generation  $g$ , for each  $\theta_{i,g}$ , the differential evolution picks a random subgroup of three distinct points, different from  $\mathbf{x}_{i,g}$ , labeled by  $r_0, r_1, r_2$  within the corresponding population, and a new point is created as:

$$\mathbf{v}_{i,g} = \theta_{r_0,g} + F(\theta_{r_1,g} - \theta_{r_2,g}) \quad (C1)$$

where  $F \in [0, 1]$  is an hyperparameter that must be set. Notice that  $\mathbf{v}_{i,g}$  can be seen as  $\theta_{r_0,g}$  after being affected by a mutation. A new candidate point  $\mathbf{u}_{i,g}$  is created from the coordinates of  $\theta_{i,g}$  and  $\mathbf{v}_{i,g}$  choosing each one randomly between the two, independently. This crossover phase aims at creating an off-spring candidate that has the features of both its parents. Finally,  $\mathbf{u}_{i,g}$  and  $\theta_{i,g}$  compete with each other, and if  $EI(\mathbf{u}_{i,g}) \geq EI(\theta_{i,g})$   $\theta_{i,g}$  is replaced, otherwise is kept. Once this procedure is performed for every point in the generation  $g$ , a population of  $N_P$  winner points is obtained, and one iteration is completed. The algorithm iterates for  $N_T$  times until the standard deviation of the population energy is below a certain threshold (Fig. 6(e)). When the threshold criterion is met, the point with the maximum energy is selected as solution.

In a flat landscape, it may happen that the algorithm stops because all the points have approximately the same energy but are still far apart from each other. To solve this problem, we modified the convergence parameters including a threshold on the average distance between points, as plotted in Fig. 6(f) during training. This increases the number  $N_T$  of iterations of the algorithms but guarantees that the points do not get stuck on a plateau and keep looking for a candidate maximum. The efficiency of the differential evolution search is driven by its simple update rule between generations. However, it is costly in terms of number of calls of the acquisition function as shown also in the results in the paper.

### Appendix D: Other optimizers

*Basin-hopping*— Basin-hopping is a global stochastic optimization algorithm [28]. It combines two steps: (i) a local optimization which proposes a candidate solution and (ii) a perturbation of such candidate in order to make it hop to other basins which might contain a global optimal point. The new point is accepted or rejected according to a probability which depends on a “temperature” parameter. The “temperature” parameter decreases with the iteration number so that, at the beginning, new proposals are easily accepted while, at larger iterations, the algorithm becomes more and more selective. The algorithm runs for a fixed number of iterations.

*Dual annealing*— This global optimization algorithm is the generalized form of the simulated annealing and it is paired with a local optimization which is performed at the end of the annealing to refine the solution [29]. It is a variation of a hill climbing algorithm in which a solution is randomly perturbed and the new proposed point is accepted with a probability that depends on the difference in energy between the two points. This probability also

depends on a “temperature” parameter that, like in the

basin-hopping case, decreases with the number of iterations in order to converge to a candidate solution.